

**Experimental and theoretical cross sections for elastic electron scattering from zinc**

B. P. Marinković, R. Panajotović, and D. Šević

*Institute of Physics Belgrade, University of Belgrade, Pregrevica 118, 11080 Belgrade, Serbia*

R. P. McEachran

*Plasma Research Laboratories, Research School of Physics and Engineering, Australian National University, Canberra, ACT 0200, Australia*

G. García

*Instituto de Física Fundamental, CSIC, Serrano 113-bis, E-28006 Madrid, Spain*

F. Blanco

*Departamento de Estructura de la Materia, Física Térmica y Electrónica, Universidad Complutense de Madrid, Avenida Complutense, E-28040 Madrid, Spain*

M. J. Brunger\*

*College of Science and Engineering, Flinders University, G.P.O. Box 2100, Adelaide, South Australia 5001, Australia*

(Received 11 March 2019; published 10 June 2019)

We report on experimental elastic differential and integral cross sections for electron scattering from zinc. The energy range of these measurements is 10–100 eV, while the scattered electron angular range in the differential cross-section data is  $10^\circ$ – $150^\circ$ . We also supplement our measured data with applications of our optical potential and relativistic optical potential approaches to this problem. Where possible, the present results are compared against those from earlier B-spline R-matrix [O. Zatsarinny and K. Bartschat, *Phys. Rev. A* **71**, 022716 (2005)] and convergent close coupling [D. V. Fursa, I. Bray, R. Panajotović, D. Šević, V. Pejčev, D. M. Filipović, and B. P. Marinković, *Phys. Rev. A* **72**, 012706 (2005)] computations. Good overall qualitative accord is typically observed.

DOI: [10.1103/PhysRevA.99.062702](https://doi.org/10.1103/PhysRevA.99.062702)**I. INTRODUCTION**

There appear to be two main reasons for why studies of electron-zinc (Zn) scattering processes are important. The first is fundamental, in that Zn represents a quasi-two-electron atom for which a target description of a [core]ns<sup>2</sup> configuration has been previously quite successful in describing scattering phenomena from similar targets such as helium [1], beryllium [2], and magnesium [3]. As a consequence, testing this representation on a heavier atom, where relativistic effects might be important, is a valid rationale for its study. The second reason is applied, and largely stems from the work of Born [4,5], who suggested that Zn might be an attractive replacement for mercury in making high-pressure gas discharge lamps more environmentally friendly. More recently, studies on the emission dynamics of an expanding ultrafast laser-produced Zn plasma have been reported [6,7]. In the latter of those studies, Gupta *et al.* [7] detailed a collisional radiative model, using relativistic distorted wave (RDW) cross-section calculation results, in order to interpret the data of Smijesh and Philip. [6]. That collisional radiative model included the RDW elastic integral cross section (ICS),

as well as the ICSs for discrete inelastic processes, to ensure that the sum of their individual ICSs was consistent with the total cross section and therefore that their [7] cross-section data base was self-consistent. As a consequence of the Born [4,5] work, White *et al.* [8] conducted an initial multiterm simulation study looking at the transport characteristics of a swarm of electrons drifting through a background Zn vapor under the influence of an external electric field. That work of White *et al.* [8] demonstrated that anisotropic scattering, through incorporation of the elastic momentum transfer cross section [8] of Zn, was necessary for accurately describing the electron transport characteristics in Zn under the influence of such an applied (external) electric field.

Previous studies into electron-zinc scattering, particularly in regard to measurements, have been somewhat limited. Experimental excitation cross sections, for the  $4^1P$  and  $5^1P$  states in Zn, have been reported by Williams and Bozinis [9], Panajotović *et al.* [10], and Fursa *et al.* [11]. Measurements of coherence and correlation parameters for the  $4^1P$  state have also been published by Piwiński *et al.* [12]. To the best of our knowledge, only a limited study of elastic cross sections for scattering from the  $4^1S$  state of Zn is available in the literature [9] and improving that situation thus forms an important rationale for the current investigation. Having said that, we do also note two early conference papers from Trajmar and Williams

\*Corresponding author: michael.brunger@flinders.edu.au

[13] and Predojević *et al.* [14]. The situation with respect to theory is a little better, with earlier elastic computations from Childs and Massey [15], McGarrah *et al.* [16], and Kumar *et al.* [17] being noted. As those earlier computations have been largely superseded, we do not discuss them further. More recently, a R-matrix result (incorporating 23 target states) [8], a B-spline R-matrix (BSR) approach [18] (incorporating 49 target states), and a convergent close-coupling (CCC) method [11] (incorporating 206 target states) have become available in the literature. While the CCC results were only reported in Fursa *et al.* [11] for the  $4^1P$  and  $5^1P$  states, elastic results were also obtained as a part of that computation. Nonetheless, with an eye to ultimately formulating a recommended database for electron-Zn scattering [19], further calculations in the form of our optical potential (OP) and relativistic optical potential (ROP) methods have been undertaken here. Broadening of the available theoretical results was thus another important rationale for the present paper.

It is well known in the electron-scattering community that the pioneering electron-metal vapor measurements, made at the Jet Propulsion Laboratory (JPL) from the early 1970's to the early 1980's, for both elastic and discrete inelastic processes, have not stood the test of time and are inaccurate. This has been confirmed by both independent measurements from other groups and by theory, with examples for sodium [20], magnesium [21–23], and lead [24], to name but a few systems, being given here in support of our assertion. The review of Bartschat [25] might also be consulted. Therefore, a further rationale of the present paper was to explicitly check this for elastic scattering in zinc [9] and, just as importantly, to extend the available cross-section data to energies beyond 40 eV, which is presently the only energy available in the literature. This is crucial for providing a serious benchmark to test theory against.

The atomic, molecular, and optical physics scattering community has, for some time now, been endeavoring to compile accurate and complete cross-section data bases [26] for scattering systems relevant to simulating charged-particle behavior in, for example, electron swarm systems [27–29] and radiation damage in matter [30–32], and for understanding the role of electron-driven processes in planetary atmospheres [33,34]. The importance of elastic-scattering cross sections, which do not deposit energy in the background medium or excite states leading to photon emission that can be analyzed for diagnostic purposes [35], has probably been somewhat undervalued by that community. In fact, by allowing for anisotropy in electron swarm transport through the momentum transfer cross section [27–29] and, through the elastic differential cross sections (DCSs) [30–32], looking at the dispersion of the electrons as they travel through the body, the elastic-scattering process is crucial for a quantitative description of those phenomena. This forms a further allied rationale for this paper.

The remainder of this paper is structured as follows. In the next section we present a brief discussion of our experimental apparatus and methods, while in Sec. III details of our OP and ROP calculations are provided. Our results and a discussion of those results are given in Sec. IV, with some conclusions from the present investigation thereafter being drawn.

## II. EXPERIMENTAL DETAILS

The apparatus is the same as that used in our earlier inelastic electron-Zn measurements [10,11], so that only a brief description is needed here. It consists of a conventional crossed-beam spectrometer, with hemispherical energy selectors in both the monochromator and analyzer. Note that both these selectors were fabricated from molybdenum. The electron beam was transported and focused by a series of cylindrical-symmetry lenses, that were made of gold-plated oxygen-free high thermal conductivity copper. A “zoom” lens was situated at the exit of the monochromator, in order to provide a stable focus at the interaction region for the electron energy range of interest to this paper, specifically, for incident electron energies between 10 and 100 eV. Note that the incident electron-beam current was in the range 1–10 nA for the present experiments, as measured using a standard Faraday cup configuration, while the current energy resolution was  $\sim 40$ -meV full width at half maximum (FWHM).

In all crossed-beam scattering experiments it is crucial to minimize the value of the Earth's magnetic field in the system, and particularly at the interaction region. This is to ensure that the paraxial focusing properties of the incident and scattered electron beams are maintained. In this case the residual magnetic field in the interaction region was measured to be less than  $0.1 \mu\text{T}$ , with this being achieved by utilizing double  $\mu$ -metal shielding.

The energy scale was calibrated by measuring the position of the well-known [36,37]  $(4s4p^2)^2D$  resonance in the elastic channel, located at 4.25 eV [37]. Due, at least in part, to the asymmetry of this feature, we estimate the uncertainty on this calibration to be  $\sim \pm 300$  meV. The position of the true zero-scattering angle was determined before each angular distribution measurement, by checking the symmetry of the scattered electron signal at positive and negative angles with respect to the unscattered electrons. The uncertainty in the angular scale was  $\pm 0.5^\circ$ , while the overall angular resolution of the present experimental configuration was  $1.5^\circ$  (FWHM). Note that the analyzer could be rotated from  $-30^\circ$  to  $+150^\circ$  with respect to the primary electron beam.

The atomic zinc beam, formed from ultrapure zinc granules, was produced using a resistively heated oven made of titanium. The oven nozzle aspect ratio was 0.075, a small enough value that should assist in minimizing any possible effective-path-length correction factor effects on the measured angular distributions even for a single-tube capillary such as here [38,39]. Nonetheless, when required, the appropriate effective path-length correction factor for our scattering geometry, from Brinkman and Trajmar [38], was employed. Monitoring of the temperature at both the top and bottom of the crucible was necessary in order to provide stable conditions for the target Zn beam. A higher temperature at the top of the crucible ensured the nozzle did not clog, while a somewhat lower, but constant, temperature ( $\sim 670$  K) at the bottom provided the effusive flow of the atomic beam. The corresponding metal vapor pressure was approximately 10 Pa, while the background pressure in the chamber was better than 5 mPa.

Irrespective of the incident electron energy ( $E_0 = 10, 15, 20, 25, 40, 60, 80, \text{ or } 100$  eV), our elastic angular distribution measurements were only undertaken when stable

TABLE I. Present measured  $4^1S(\text{EL})/4^1P(4P)$  ratios at  $10^\circ$  and  $20^\circ$  scattering angles and for energies between 10 and 100 eV. Also shown are the relevant  $4^1P$  DCSs from [10,11] and our corresponding OP and ROP theory results. Note that EL denotes the elastic channel.

DCS	Scattering angle		20°					10°		
	10 eV	15 eV	20 eV	25 eV	40 eV	40 eV	60 eV	80 eV	100 eV	
4P [10,11] ( $10^{-16}$ cm <sup>2</sup> /sr)	2.1	2.64	2.52	1.92	0.644	13.7	6.69	5.92	3.61	
EL/4P experiment	$8.3 \pm 1.9$	$3.5 \pm 0.5$	$2.15 \pm 0.25$	$1.77 \pm 0.42$	$1.8 \pm 0.7$	$0.76 \pm 0.16$	$0.58 \pm 0.07$	$0.86 \pm 0.10$	$1.06 \pm 0.07$	
EL experiment ( $10^{-16}$ cm <sup>2</sup> /sr)	$17.4 \pm 5.9$	$9.24 \pm 2.09$	$5.41 \pm 1.21$	$3.40 \pm 0.99$	$1.15 \pm 0.52$	$10.5 \pm 4.7$	$3.88 \pm 1.11$	$5.07 \pm 1.48$	$3.82 \pm 1.04$	
EL OP ( $10^{-16}$ cm <sup>2</sup> /sr)	10.8	7.81	5.74	4.31	2.39	10.8	9.41	8.82	8.42	
EL ROP ( $10^{-16}$ cm <sup>2</sup> /sr)	15.3	10.2	6.93	4.87	2.07	14.3	10.8	8.92	7.82	

electron-beam and zinc-beam operating conditions were achieved. The angular distributions for elastic scattering, i.e., when the energy loss of the incident beam after scattering was equal to 0 eV, at each energy, were measured by recording the number of true elastic-scattering events as a function of the scattered electron angle. Note that background electron scattering from the residual gas in our scattering chamber was carefully monitored, and was found to be very small across most of the scattered electron angular range of this investigation. Further note that those relative angular distribution data were corrected for the effective path-length factor [38] before normalization. Due to interference from the primary electron beam, in practice the minimum scattered electron angle that we could access was  $\theta = 20^\circ$  for  $E_0 \leq 25$  eV and  $\theta = 10^\circ$  for  $40 \text{ eV} \leq E_0 \leq 100$  eV. On the other hand, the maximum scattered electron angle we could measure, at all energies studied, was  $\theta = 150^\circ$ . In this case the restriction was caused by the physical size of the monochromator and analyzer and their associated electron-optic lens elements. The present angular distributions, again at each energy, were subsequently placed on an absolute scale, from energy-loss measurements that encompassed the elastic ( $4^1S$ ) and inelastic ( $4^1P$ ) peaks at certain specific normalization angles. From the ratio of the elastic to inelastic intensities, in the energy-loss spectrum, at the normalization angle, and a knowledge of the absolute  $4^1P$  DCSs from Fursa *et al.* [11], our angular distribution measurement at the given energy could now be placed on an absolute scale. Examples for this approach, at scattered electron angles of  $10^\circ$  and  $20^\circ$  and for all our incident electron energies between 10 and 100 eV, are given in Table I. Also included in this table are the relevant  $4^1P$  DCSs from [10,11] and our corresponding OP and ROP theoretical results (see later).

The only concern with this approach, particularly at the lower incident electron energies, is the behavior of the analyzer transmission as a function of the scattered electron energy. This follows as the energy gap between the  $4^1S$  and  $4^1P$  states is  $\sim 5.8$  eV [18], so that for a 15-eV incident electron the outgoing scattered electron energies will vary from 15 eV ( $4^1S$  state) to 9.2 eV ( $4^1P$  state) across our energy-loss spectrum. However, our analyzer electron optics were specifically designed to cope with such situations so that we believe our transmission function is uniform to better than 23% at 10 eV and 7% at 100 eV.

An alternative approach, at each energy, that we employed here was to measure energy-loss spectra at each scattered electron angle and, in the manner just discussed, determine the elastic DCS directly from those energy-loss spectra. The beauty here is that the effective path-length correction factor cancels out in taking the ratio, and is thus of no concern with that approach. However, the analyzer transmission function issue (as just discussed) remains open. In any event, the elastic DCSs we determined from these two approaches, irrespective of the incident electron energy, were always consistent to within the uncertainties we cite. This gives us some confidence in the efficacy of our experimental measurement techniques and procedures. A summary of the present measured elastic DCSs and their uncertainties is given in Table II, with plots of those results and our new OP and ROP computations being found in Figs. 1 and 2. Having obtained our elastic DCSs, we now wish to extrapolate them to  $0^\circ$  and  $180^\circ$ , perform an interpolation, and then undertake the usual integration in order to derive elastic ICSs at each energy. To accomplish this in the least subjective manner possible, we applied the complex phase-shift analysis approach originally developed by Allen and coworkers [40,41]. Full details of this method can be found in [40,41], but essentially the user inputs the relevant beam energy and the dipole polarizability of zinc ( $38.8 a_0^3$  [42] in this case), the number of complex phase shifts (e.g.,  $s$ ,  $p$ , and  $d$  waves) to be varied in order to minimize the difference between the measured and simulated DCSs, and finally the maximum value of the partial waves to be employed in the Born expansion that accounts for the higher-order partial waves. In all cases the functional form of Allen and coworkers [40,41] produced an excellent representation of the measured DCSs, so that we are confident in the validity of the ICSs we have derived from this approach. The present experimental and theoretical elastic ICSs can be found in Table III and Fig. 3. The uncertainties on our measured DCSs stem from several contributions. The stabilities of the electron and atomic beams are both better than 2% over the lifetime of a given experimental run. Despite the large dynamic range of the elastic intensity over the scattered electron angles we probed (see Table II), the statistical uncertainties in our angular distributions were rarely worse than 30% and only then at the higher scattering angles. To place the angular distributions on

TABLE II. Experimental differential cross sections and absolute uncertainties (in parentheses) in units of  $10^{-16}$  cm<sup>2</sup>/sr for elastic electron scattering from the ground state of zinc. Uncertainties are at the one standard deviation level.

Angle	10 eV	15 eV	20 eV	25 eV	40 eV	60 eV	80 eV	100 eV
10					10.5(4.7)	3.88(1.11)	5.07(1.48)	3.82(1.04)
15	19.5(9.9)		11.1(2.5)	8.46(2.48)	3.61(1.62)			
20	17.4(5.9)	9.24(2.09)	5.41(1.21)	3.40(0.99)	1.15(0.52)	0.606(0.190)	0.646(0.210)	0.532(0.157)
25			2.46(0.55)	1.35(0.40)	0.343(0.154)			
30	6.02(2.03)	2.41(0.54)	1.05(0.24)	0.530(0.155)	0.096(0.043)	0.065(0.025)	0.074(0.030)	0.090(0.031)
35			0.447(0.099)	0.198(0.058)	0.020(0.009)			
38					0.0075(0.0035)			
40	2.05(0.69)	0.618(0.140)	0.184(0.041)	0.055(0.017)	0.0087(0.0040)	0.031(0.014)	0.064(0.027)	0.056(0.020)
45		0.261(0.059)	0.067(0.015)	0.0071(0.0025)	0.026(0.012)			
48				0.0037(0.0013)				
50	0.668(0.226)	0.106(0.024)	0.011(0.003)	0.0045(0.0016)	0.047(0.021)	0.056(0.023)	0.092(0.037)	0.064(0.023)
55	0.365(0.124)	0.043(0.010)	0.0053(0.0013)	0.020(0.006)	0.059(0.026)			
60	0.163(0.056)	0.016(0.004)	0.011(0.002)	0.034(0.010)	0.062(0.028)	0.071(0.028)	0.075(0.031)	0.044(0.017)
65	0.074(0.026)	0.0063(0.0017)	0.017(0.004)	0.043(0.013)	0.060(0.027)			
70	0.029(0.011)	0.0040(0.0013)	0.023(0.005)	0.044(0.013)	0.050(0.022)	0.022(0.010)	0.026(0.012)	0.019(0.008)
75		0.0040(0.0012)	0.026(0.006)	0.038(0.012)				
80	0.011(0.005)	0.0060(0.0017)	0.026(0.006)	0.031(0.009)	0.024(0.011)	0.015(0.008)	0.0061(0.0032)	0.0052(0.0025)
85	0.018(0.007)	0.0082(0.0022)	0.027(0.005)	0.026(0.008)				
90	0.031(0.011)	0.0099(0.0026)	0.020(0.005)	0.019(0.006)	0.0093(0.0043)	0.0066(0.0039)	0.0094(0.0046)	0.0070(0.0032)
95			0.017(0.004)	0.013(0.004)				
100	0.055(0.020)	0.017(0.004)	0.015(0.003)	0.0088(0.0029)	0.0062(0.0029)	0.018(0.009)	0.023(0.010)	0.016(0.007)
105			0.012(0.003)	0.0058(0.0020)				
110	0.090(0.031)	0.026(0.006)	0.014(0.003)	0.0047(0.0016)	0.0089(0.0041)	0.024(0.011)	0.031(0.013)	0.025(0.010)
115			0.017(0.004)	0.0070(0.0023)				
120	0.112(0.039)	0.041(0.010)	0.022(0.005)	0.0092(0.0029)	0.012(0.006)	0.027(0.012)	0.042(0.017)	0.023(0.010)
125			0.031(0.007)	0.013(0.004)				
130	0.148(0.051)	0.064(0.015)	0.043(0.010)	0.019(0.006)	0.011(0.005)	0.025(0.011)	0.023(0.010)	0.013(0.006)
135			0.060(0.013)	0.030(0.009)				
140	0.184(0.063)	0.095(0.022)	0.082(0.018)	0.043(0.013)	0.016(0.007)	0.010(0.006)	0.0070(0.0035)	0.0062(0.0028)
145			0.110(0.025)	0.061(0.018)				
150	0.253(0.086)	0.143(0.033)	0.145(0.032)	0.085(0.025)	0.035(0.016)	0.0077(0.0043)	0.0032(0.0019)	0.0013(0.0008)

an absolute scale, we carry over the intrinsic uncertainty on the  $4^1P$  DCS at the normalization angle, the uncertainty in our effective path-length correction factor ( $<5\%$ ), the uncertainty of  $\sim 10\%$  in our energy and angular calibrations, and the uncertainty of  $23\%$  at 10 eV decreasing to  $7\%$  at 100 eV

TABLE III. Present elastic ICS ( $\times 10^{-16}$  cm<sup>2</sup>), as derived from our measured DCS, for electron scattering from Zn. Estimated uncertainties in our data are  $\pm 35\%$ , and are at the one standard deviation level. Note that our overall estimated uncertainty includes an “extrapolation uncertainty” due to the application of our phase-shift analysis approach [40,41].

$E_0$ (eV)	ICS ( $10^{-16}$ cm <sup>2</sup> )	Absolute error ( $10^{-16}$ cm <sup>2</sup> )
10	19.22	6.73
15	13.30	4.65
20	8.61	3.01
25	6.82	2.39
40	4.27	1.49
60	2.23	0.78
80	3.28	1.15
100	2.63	0.92

on our analyzer transmission function associated with the energy-loss measurements and our determination of the elastic to inelastic ratios. When combining all these contributions in quadrature, we found that the overall uncertainties on our elastic DCSs lay in the range  $\sim 22\text{--}62\%$ , with the exact uncertainties being found in Table II. For our elastic ICSs we estimate their uncertainties to be a conservative  $\pm 35\%$ .

### III. THEORETICAL METHODS

As already mentioned above we have employed two different theoretical approaches to calculate the elastic differential and integral cross sections of this investigation. These are now briefly detailed below.

#### A. OP approximation

We have recently described, in some detail, our optical potential approach as applied to the electron-beryllium [2] and electron-magnesium [3] scattering systems. All the generic details of our atomic OP method, that we gave in these papers, are equally applicable here and so as a consequence we do not repeat them. Rather, we simply highlight that when our OP method was benchmarked against a sophisticated BSR calculation [43], for elastic electron scattering from iodine,

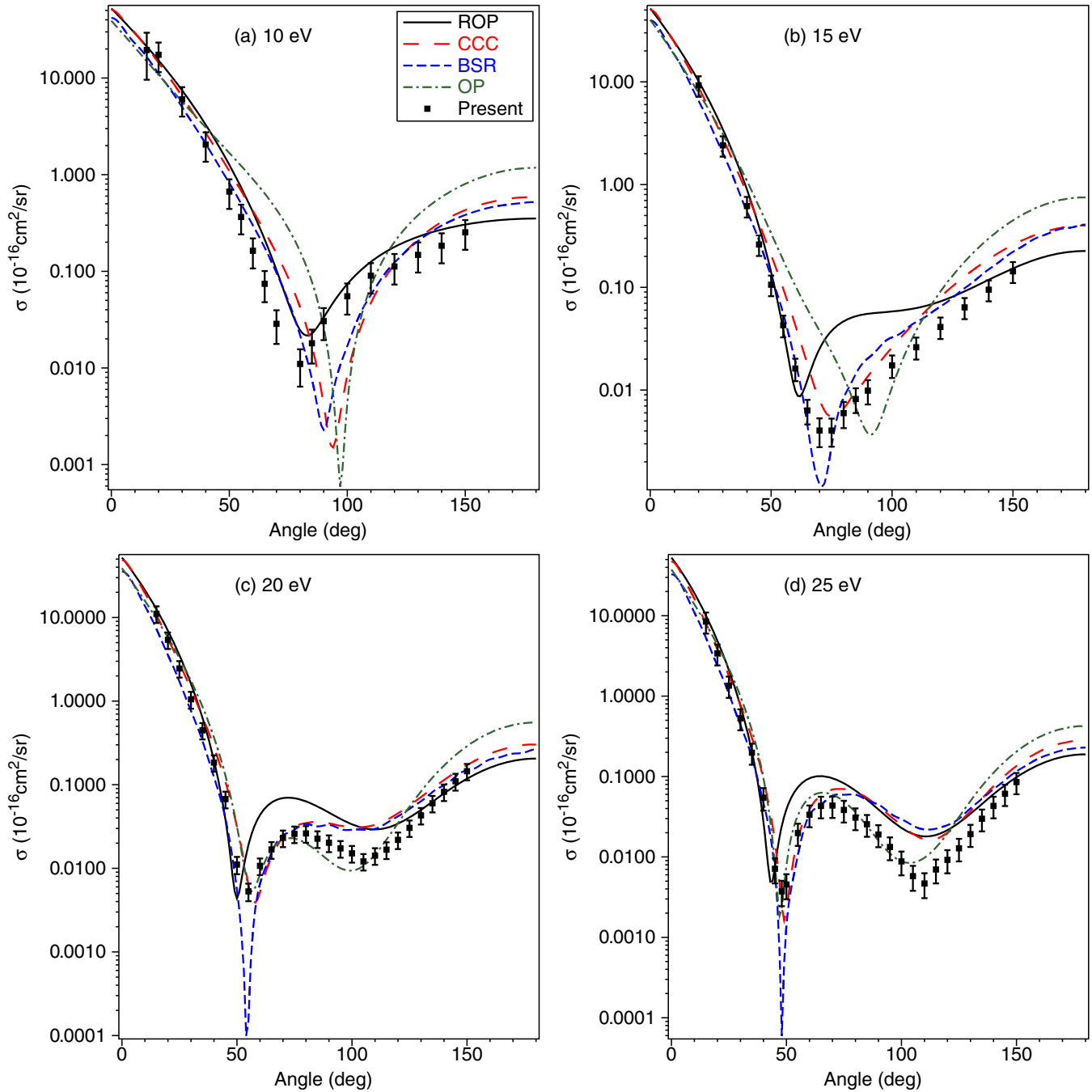


FIG. 1. Differential elastic cross sections ( $\times 10^{-16}$  cm<sup>2</sup>/sr) for electron scattering from zinc at (a) 10 eV, (b) 15 eV, (c) 20 eV, and (d) 25 eV. The present measurements (■) and OP (— · — · —) and ROP (—) calculations are compared against earlier CCC (---) [11] and BSR (- - - -) [18] theory results. See also the inset.

very good agreement was found between them. We therefore anticipate that it will provide a good description for the elastic-scattering process in Zn as well.

### B. ROP theory

We also gave a detailed synopsis of our relativistic optical potential calculations in [2,3], so we do not repeat them again now. In this case, however, there are some details pertaining specifically to the relativistic optical potential employed for Zn, which we now provide. In this paper the elastic and absorp-

tion cross sections were calculated using a complex relativistic optical potential (ROP) method in a similar manner, as just noted, to that outlined in the recent papers [2,3] for Be and Mg. A complete description of the ROP method is given in [44]; this paper will be referred to as paper I hereafter.

The ROP method is based upon the solution of the Dirac scattering equations which contain both static and polarization potentials, the exchange terms, and a nonlocal absorption potential to account for excitation and ionization processes. The ground- and excited-state wave functions of zinc were determined in a single configuration calculation using the

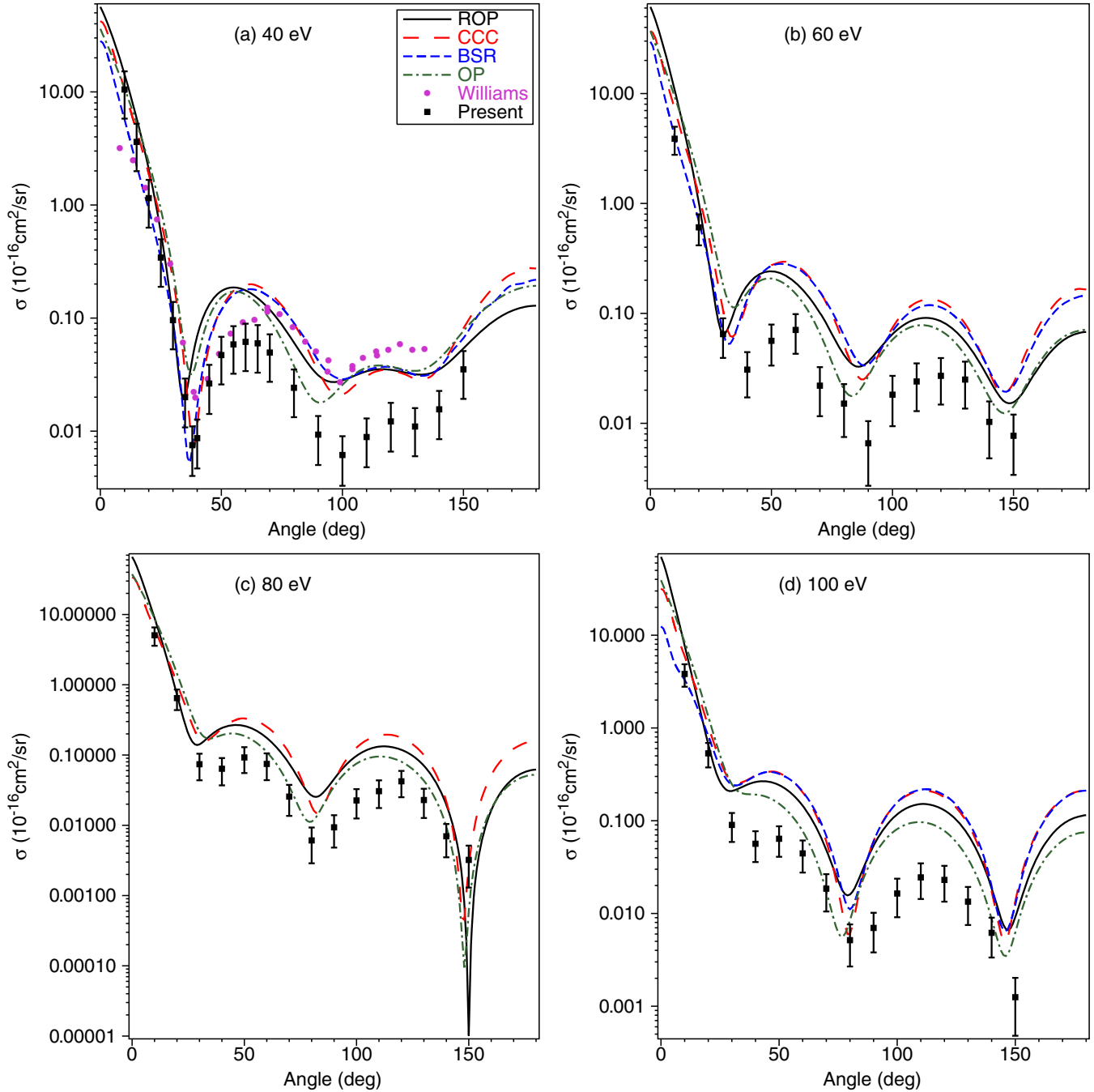


FIG. 2. Differential elastic cross sections ( $\times 10^{-16}$  cm<sup>2</sup>/sr) for electron scattering from zinc at (a) 40 eV, (b) 60 eV, (c) 80 eV, and (d) 100 eV. The present measurements (■) and OP (— · — · —) and ROP (—) calculations are compared against earlier CCC (— —) [11] and BSR (· · · ·) [18] theory results. Also plotted is the measurement of Williams and Bozinis (●) [9] at 40 eV. See also the inset.

multiconfiguration Dirac-Fock program of Grant *et al.* [45]. The static potential was determined in the usual manner from the ground-state Dirac-Fock orbitals of zinc, while the nonlocal exchange interaction was included by antisymmetrizing the total scattering wave function. The polarization potential was determined by the polarized-orbital method of McEachran *et al.* [46,47] and included the first seven multipole potentials plus the corresponding dynamic polarization potential [48]. Thus, asymptotically the polarization potential contained all terms up to and including those corresponding to  $r^{-14}$ .

The nonlocal absorption potential was determined as an expansion over the inelastic channels of the target atom. These inelastic channels include both excitation of the higher-lying bound states as well as the single ionization of the target as given by Eq. (21b) of paper I. Also included were those channels which correspond to the ionization of 3*p* and 3*d* electrons at approximately 17 and 75 eV, respectively. For the excited bound states of zinc, which were used in the absorption potential, we included those eight states where one of the electrons in the outer 3*s* valence shell was excited to a higher-lying  $np^{1,3}P$  state with  $n = 4$  to 7 inclusive.

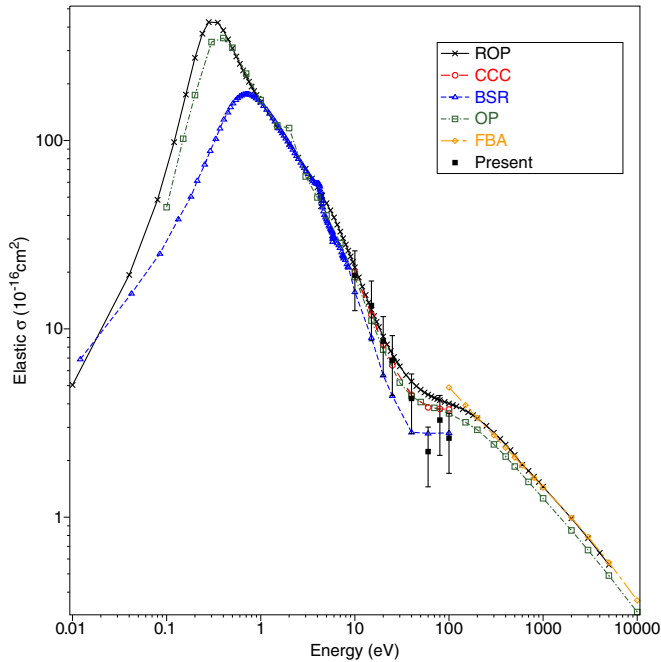


FIG. 3. Integral elastic cross sections ( $\times 10^{-16}$  cm $^2$ ) for electron scattering from zinc. The present measurements ( $\blacksquare$ ) and OP ( $\square$ ) and ROP ( $\times$ ) calculations are compared against earlier CCC ( $\circ$ ) [11], BSR ( $\triangle$ ) [18], and FBA ( $\diamond$ ) [51] theory results. See also the inset.

For the case of ionization, we included those continuum states which correspond to an orbital angular momentum of zero to four; this gives rise to up to 71 ionization channels depending on the total angular momentum of the incident electron.

All the present OP and ROP results are converged and so have an intrinsic uncertainty of less than 1%. However, in terms of their ability to accurately reproduce benchmarked data or sophisticated CCC and BSR results, our experience [2,3,43] suggests an uncertainty of  $\sim 10\%$  for energies above about 1 eV and an uncertainty of up to  $\sim 50\%$  for energies below 1 eV. That larger uncertainty at those lower energies is due to the existence of the low-energy resonance (see Fig. 3), which can only be approximately represented in the OP and ROP methods. For these optical potential methods to compete with results from CC methods here, we would need to include the excited states involved in the resonance, in momentum space, and treat it as we do the ground state. The large basis sets in the BSR and CCC methods should give a good representation of both states involved in the resonance, as well as give a good representation of the polarization interaction. Therefore, large basis set BSR and/or CCC calculations, if available, should be preferred below  $\sim 0.5$  eV.

#### IV. RESULTS AND DISCUSSION

In Table II and Figs. 1 and 2 we show the results from our experimental differential cross-section measurements for elastic scattering from the  $4^1S$  ground state of Zn. Also shown in Figs. 1 and 2 are the results from our present optical potential and relativistic optical potential DCS computations, and the earlier theoretical CCC and BSR cal-

culations. As noted by Bartschat [49], the BSR results of Zatsarinny and Bartschat [18] focused on the lower-energy scattering phenomena. As a consequence, at higher energies some convergence problems (recall this is only a 49-state calculation) might be anticipated to be encountered. This is indeed the case; several of the higher-energy BSR elastic differential cross sections exhibit unphysical (although subtle) oscillations in their angular distributions. All the experimental and theoretical angular distributions exhibit a strong forward peaking (i.e., at smaller scattering angles) in their absolute elastic cross-section magnitudes (see Figs. 1 and 2) with this degree of forward peaking increasing as the incident electron energy increases. This behavior is consistent with the important role that zinc's strong dipole polarizability [42] plays in the scattering dynamics of this collisional system. Also of general note is that the number of local minima in the DCSs increases as the incident electron energy increases. Specifically, at 10 and 15 eV we observe one local cross-section minimum, while at 20 and 25 eV there are two local minima in the DCS and for energies of 40 eV and above there are three local minima. In this case the oscillatory behavior in the angular distributions, both experimental and theoretical, is physical and reflects the interference between the various phase shifts that describe elastic scattering in this system at a given energy. It is worthy of note that the positions of these minima in the angular distributions, although not necessarily their depths, are probably best described by the CCC and our OP theories (again see Figs. 1 and 2). Finally, in a general sense, we note that electron exchange also plays an important role, particularly at the lower energies, in this system. The best way to ascertain this is to “turn off” exchange in our computations, and to observe the effect that this unphysical action has on the calculated DCS (not explicitly shown in Figs. 1 and 2). As just noted, that effect was important at the lower energies of this paper.

Considering Fig. 1(a) in more detail we see that the present ROP result probably best describes the measured data, in terms of the shape, magnitude, and angular position of the DCS minimum. Nonetheless, it is fair to note that all the computations at least qualitatively reproduce the gross features of this elastic DCS. At 15 eV, however, the situation has changed a little with the CCC result [11] now best representing the measured DCS [see Fig. 1(b)]. However, we would again characterize the level of accord between the available theories and our data as being fair overall. By 20 eV [see Fig. 1(c)] best agreement between the measured data and theory is probably afforded by our OP result, although both the CCC [11] and ROP theories also do reasonable jobs in reproducing the qualitative features of this elastic DCS. Only the BSR computation [18], which predicts a far deeper cross-section minimum than any of the other theories or experiments at this energy, has significant problems here. This may reflect some issues with their convergence, as Bartschat noted [49], and indeed if we look closely at Fig. 1(c) we can see some small (unphysical) oscillations in their [18] angular distribution. A similar story to that just outlined at 20 eV can be found in Fig. 1(d) for 25 eV. Hence we do not consider that energy further.

At 40 eV, in Fig. 2(a), there is an earlier elastic DCS measurement from Williams and Bozinis [9] available in

the literature. When we compare that result to the present measurements we find, to within their stated uncertainties, very good agreement between them for scattered electron angles less than about  $70^\circ$ . Above  $70^\circ$ , however, the data of Williams and Bozinis [9] are significantly higher in magnitude than the present DCS, and in better accord with all the theory results. As noted previously, electron-metal vapor measurements made at JPL from the early 1970's to the early 1980's are now known to be inaccurate. Hence our observations regarding the level of agreement between our 40-eV measurements and those of Williams and Bozinis [9], in Fig. 2(a), are not particularly surprising, but were important to confirm. Figure 2(a) also indicates that it is the CCC result [11] that is probably in best overall agreement with our measured DCS, although our OP calculation also does a fair job in qualitatively reproducing the features of the 40-eV angular distribution. Once again, we find some suggestion of convergence problems with the BSR computation [18,49]. In Fig. 2(b) we present our 60-eV results. At this energy all the theories well reproduce the angular structure in this elastic DCS, although in terms of the cross-section magnitude for scattering angles greater than about  $30^\circ$  they are all much stronger in magnitude than our measured data. A similar story to that just outlined for 60 eV is also found at 80 eV [Fig. 2(c)] and 100 eV [Fig. 2(d)]. Indeed it is fair to say that for incident electron energies greater than 25 eV all the DCSs found in various theories are larger in magnitude than our measured results at middle and backward scattered electron angles. This observation is not new to us, having been seen in all our recent electron-molecule scattering studies [50]. In essence it is indicative of the “flux competition” between the open elastic, discrete inelastic, and ionization channels at a given incident electron energy. Assuming our measured DCSs are in fact correct, then Figs. 1(d) and 2(a)–2(d) suggest that more flux is going into the elastic channel, compared to the discrete inelastic and ionization channels, than should be the case. However, it is worth noting that the DCSs at all these energies have magnitudes that are very small at middle and backward electron-scattering energies. Therefore it would only require a very small misapportionment of the flux into the elastic channel to lead to what we find in Figs. 1(d) and 2(a)–2(d). This highlights just how challenging these computations are, so that the level of accord that we achieve between theory and experiment in Figs. 1 and 2 is actually pretty good.

In Table III and Fig. 3 we present our derived elastic ICS for electron scattering from zinc. Also plotted in Fig. 3 are the results of our OP and ROP calculations, and corresponding CCC [11] and BSR [9] elastic ICSs. Additionally, a first Born approximation (FBA) level [26,51] calculation is also plotted in Fig. 3. The first point we can glean from Fig. 3 is the existence of a strong low-energy *p*-wave resonance feature in the elastic ICS, which is predicted by both our OP and ROP computations and the earlier BSR [18] calculation. This resonance was first observed experimentally in the electron transmission spectra (ETS) work of Burrow *et al.* [36], at an energy of 0.49 eV, with it being originally found in a semiempirical calculation by Zollweg [52] although at a slightly higher energy of 0.67 eV. The present OP calculation predicts the resonance peak at 0.4 eV, in good accord with that of Burrow *et al.* [36], while our ROP finds the peak to be

in the range 0.28–0.35 eV, which is still in fair accord with the ETS result. The 49-state BSR calculation places the peak at 0.71 eV, in better accord with the semiempirical result of Zollweg [52]. It is well known that close-coupling-type calculations, when predicting the position and peak magnitudes of these low-energy resonance features, are very sensitive to the number of channels incorporated into their computation [53]. Therefore it would be desirable if a larger basis BSR calculation were to be performed on this system. Similarly, it would be very interesting to see the CCC results [11] for incident electron energies below 10 eV and extending down to about 0.01 eV. At this stage it appears that more work needs to be done in this low-energy regime (0.01–1 eV), in order to get a better handle on the true peak energy and magnitude of this cross section. Above 1 eV, however, the situation is clearer. As can be seen in Fig. 3, for energies between 1 and 10 eV the present OP and ROP elastic ICSs are in quite good accord with the BSR result [18]. Above 10 eV, the BSR cross section becomes lower in magnitude than all of the OP, ROP, and CCC results. This observation we believe, at least in part, reflects some of the convergence issues with the BSR calculation, at the higher energies, that we discussed previously. The OP and CCC results, between 10 and 100 eV, are in excellent agreement with one another, while our ROP result, which is a little higher in magnitude in that energy range, possibly due to it incorporating relativistic effects which neither the OP or CCC computations can account for, nonetheless remains in fair accord with the OP and CCC cross sections. Finally, for energies greater than 100 eV, we note the elastic ICSs from our OP and ROP calculations and the FBA calculation [51] all exhibit the same energy dependence and are in fair accord in terms of their magnitude. It would thus be relatively easy to construct a recommended data base in that energy range by simply taking an average of the OP, ROP, and FBA ICSs.

The other major highlight in Fig. 3 is the comparison between our derived elastic ICS and the available theories, including our own, between 10 and 100 eV. Here we find a very good level of agreement between the experimental ICSs and the theoretical results from the OP, ROP, and CCC calculations, for incident electron energies between 10 and 40 eV. While this might appear a little counterintuitive, given our previous discussions of the DCSs at those energies, it can be understood as follows. Most of the contribution to the integrand of the ICSs, even allowing for the  $\sin\theta$  weighting factor, comes from the more forward electron-scattering angles of the DCSs and this is precisely where, between 10 and 40 eV, the experimental DCSs are in good accord, in the main, with those corresponding OP, ROP, and CCC computations. At higher energies (60–100 eV), however, the measured (derived) ICSs are lower in magnitude than the OP, ROP, and CCC results (see Fig. 3), and in better accord with the BSR calculated ICS. Given our previous discussion in relation to some possible convergence problems with the BSR at higher energies, that agreement between our experimental ICS and the BSR ICS must be considered to be a little serendipitous. Again, this ICS behavior at higher energies fully reflects the higher-energy DCS results (see Fig. 2). Specifically, the forward angle DCSs at those energies (except in part at 80 eV) are all a little lower in magnitude than the OP, ROP, and CCC cross sections

with this observation then being carried through, as one would expect, to the ICS level results (see Fig. 3).

## V. CONCLUSIONS

We have reported on original differential cross-section measurements for elastic electron scattering from zinc. The energy range of those experiments was 10–100 eV, with the scattered electron angular range being 10°–150°. From those data we employed our phase-shift analysis procedure to derive corresponding integral cross sections. In addition, theoretical results from our optical potential and relativistic optical potential computations were also reported. On the basis of the work of McEachran and Stauffer [54] and Bartsch *et al.* [55], with polarized electrons, we had anticipated relativistic effects in Zn ( $Z=30$ ) to be modest but nonetheless observable. Unfortunately, perhaps due to the slightly different representations of polarization, exchange, and the absorption interaction between our OP and ROP formalisms, no such effects were quantified in this investigation. This suggests that for a target even with  $Z=30$  it may be too light to elucidate relativistic effects with unpolarized electrons. Where possible the present DCS and ICS experimental and theoretical data were compared against those from earlier CCC and BSR calculations. At the DCS level we found good qualitative accord between our measurements and the available calculations, although at the higher (40–100 eV) incident electron energies the theories tended to be systematically higher in magnitude than our measured results at middle and backward angles. This we believe was due to a small misapportionment of flux in the theory between the elastic channel and the discrete inelastic and ionization channels (i.e., flux competition). In particular, the results embodied in Figs. 1 and 2 indicate just how difficult it is for theory to describe a scattering process where the cross sections vary by four to five orders of magnitude over the

scattered electron angular range from 0° to 180°, the treatment of the continuum by theory being somewhat problematic in that endeavour. Nonetheless, it would be both interesting and instructive if the BSR and CCC methods were to reprise their calculations with the larger basis sets they now routinely employ with the computational power now available to them. Agreement at the elastic integral cross-section level, between theory and our measurements, was quite good across the common energy range. At lower energy ( $\leq 40$  eV), to within our stated uncertainties, the experimental ICSs were largely consistent with the CCC, BSR, OP, and ROP computations, while at higher energies, although there is a degree of good fortune here due to their convergence problems at these higher energies, the BSR cross sections are in best accord with our experimental data. While a large basis BSR calculation and an extension of the existing CCC result to lower energies ( $\sim 0.01$  eV) would be desirable, to better define the magnitude and peak energy of the  $p$ -wave resonance cross section, we nonetheless believe a plausible (recommended) elastic ICS could now be established for this scattering system and for ultimate use in simulating electron transport in gaseous zinc.

## ACKNOWLEDGMENTS

This work was financially supported, in part, by the Spanish Ministerio de Ciencia, Innovacion y Universidades (Project No. FIS2016-80440), the Australian Research Council (Projects No. DP160102787 and No. DP180101655), and the Ministry of Education, Science, and Technological Development (Project No. OI171020) of the Republic of Serbia. We thank Dr. L. Campbell for his help with some aspects of this paper, and we acknowledge helpful conversations with Prof. K. Bartschat. Finally, we also thank Dr. O. Zatsarinny and Prof. K. Bartschat for providing us tables of their BSR data and Prof. I. Bray and Prof. D. Fursa for the CCC data.

- 
- [1] D. V. Fursa and I. Bray, *J. Phys. B* **30**, 757 (1997).
  - [2] R. P. McEachran, F. Blanco, G. García, and M. J. Brunger, *J. Phys. Chem. Ref. Data* **47**, 033103 (2018).
  - [3] R. P. McEachran, F. Blanco, G. García, P. W. Stokes, R. D. White, and M. J. Brunger, *J. Phys. Chem. Ref. Data* **47**, 043104 (2018).
  - [4] M. Born, *J. Phys. D* **34**, 909 (2001).
  - [5] M. Born, *Plasma Sources Sci. Technol.* **11**, A55 (2002).
  - [6] N. Smijesh and R. Philip, *J. Appl. Phys.* **114**, 093301 (2013).
  - [7] S. Gupta, R. K. Gangwar, and R. Srivastava, Proceedings of the International Conference on Atomic Processes in Plasmas Conference, 2019 (unpublished); (private communication).
  - [8] R. D. White, R. P. McEachran, R. E. Robson, M. T. Elford, and K. Bartschat, *J. Phys. D* **37**, 3185 (2004).
  - [9] W. Williams and D. Bozinis, *Phys. Rev. A* **12**, 57 (1975).
  - [10] R. Panajotović, D. Šević, V. Pejčev, D. M. Filipović, and B. P. Marinković, *Int. J. Mass Spectrom.* **233**, 253 (2004).
  - [11] D. V. Fursa, I. Bray, R. Panajotović, D. Šević, V. Pejčev, D. M. Filipović, and B. P. Marinković, *Phys. Rev. A* **72**, 012706 (2005).
  - [12] M. Piwiński, Ł. Kłosowski, D. Dzikczek, S. Chwiroł, T. Das, R. Srivastava, A. D. Stauffer, C. J. Bostock, D. V. Fursa, and I. Bray, *Phys. Rev. A* **86**, 052706 (2012).
  - [13] S. Trajmar and W. Williams, Proceedings of the Eighth Symposium on the Physics of Ionized Gases, 1976 (unpublished), p. 199.
  - [14] B. Predojević, D. Šević, R. Panajotović, V. Pejčev, D. M. Filipović, and B. P. Marinković, Proceedings of the 20th Symposium on the Physics of Ionized Gases, 2000 (unpublished), p. 35.
  - [15] E. C. Childs and H. S. W. Massey, *Proc. R. Soc. A* **142**, 509 (1933).
  - [16] D. B. McGarrah, A. J. Antolak, and W. Williamson, *J. Appl. Phys.* **69**, 6812 (1991).
  - [17] P. Kumar, A. K. Jain, A. N. Tripathi, and S. N. Nahar, *Phys. Rev. A* **49**, 899 (1994).
  - [18] O. Zatsarinny and K. Bartschat, *Phys. Rev. A* **71**, 022716 (2005).
  - [19] L. C. Pitchford, L. L. Alves, K. Bartschat, S. F. Biagi, M.-C. Bordage, I. Bray, C. E. Brion, M. J. Brunger,

- L. Campbell *et al.*, *Plasma Process. Polym.* **14**, 1600098 (2017).
- [20] P. J. O. Teubner, J. L. Riley, M. J. Brunger, and S. J. Buckman, *J. Phys. B* **19**, 3313 (1986).
- [21] M. J. Brunger, J. L. Riley, R. E. Scholten, and P. J. O. Teubner, *J. Phys. B* **21**, 1639 (1988).
- [22] D. O. Brown, D. Cvejanović, and A. Crowe, *J. Phys. B* **36**, 3411 (2003).
- [23] B. Predojević, V. Pejčev, D. M. Filipović, D. Šević, and B. P. Marinković, *J. Phys. B* **40**, 1853 (2007).
- [24] S. D. Tošić, M. S. Rabasović, D. Šević, V. Pejčev, D. M. Filipović, L. Sharma, A. N. Tripathi, R. S. Srivastava, and B. P. Marinković, *Phys. Rev. A* **77**, 012725 (2008).
- [25] K. Bartschat, *Phys. Rept.* **180**, 1 (1989).
- [26] H. Tanaka, M. J. Brunger, L. Campbell, H. Kato, M. Hoshino, and A. R. P. Rau, *Rev. Mod. Phys.* **88**, 025004 (2016).
- [27] R. D. White, D. Cocks, G. Boyle, M. Casey, N. Garland, D. Konovalov, B. Philippa, P. Stokes, J. de Urquijo, O. González-Magaña, R. P. McEachran, S. J. Buckman, M. J. Brunger, G. Garcíá, S. Dujko, and Z. Lj. Petrović, *Plasma Sources Sci. Technol.* **27**, 053001 (2018).
- [28] Ž. Mladenovic, S. Gocić, D. Marić, and Z. L. Petrović, *Eur. Phys. J. Plus* **133**, 344 (2018).
- [29] N. Škoro, N. Puač, S. Žiković, D. Krstić-Milasević, U. Cvelbar, G. Malović, and Z. L. Petrović, *Eur. Phys. J. D* **72**, 2 (2018).
- [30] M. C. Fuss, L. Ellis-Gibbings, D. B. Jones, M. J. Brunger, F. Blanco, A. Muñoz, P. Limão-Vieira, and G. Garcíá, *J. Appl. Phys.* **117**, 214701 (2015).
- [31] P. J. Bruggeman, M. J. Kushner, B. R. Locke, J. G. E. Gardeniers, W. G. Graham, D. B. Graves *et al.*, *Plasma Sources Sci. Technol.* **25**, 053002 (2016).
- [32] I. Adamovich *et al.*, *J. Phys. D* **50**, 323001 (2017).
- [33] I. A. Mironova, K. L. Aplin, F. Arnold, G. A. Bazilevskaya, R. G. Harrison, A. A. Krivolutsky, K. A. Nicoll, E. V. Rozanov, E. Turunen, and I. G. Usoskin, *Space Sci. Rev.* **194**, 1 (2015).
- [34] L. Campbell and M. J. Brunger, *Int. Rev. Phys. Chem.* **35**, 297 (2016).
- [35] M. A. Ridenti, J. Amorim Filho, M. J. Brunger, R. F. da Costa, M. T. do N. Varella, M. H. F. Bettega, and M. A. P. Lima, *Eur. Phys. J. D* **70**, 161 (2016).
- [36] P. D. Burrow, J. A. Michejda, and J. Comer, *J. Phys. B* **9**, 3225 (1976).
- [37] J. P. Sullivan, P. D. Burrow, D. S. Newman, K. Bartschat, J. A. Michejda, R. Panajotović, R. P. McEachran, and S. J. Buckman, *New J. Phys.* **5**, 159 (2003).
- [38] R. T. Brinkman and S. Trajmar, *J. Phys. E* **14**, 245 (1981).
- [39] M. J. Brunger and S. J. Buckman, *Phys. Rep.* **357**, 215 (2002).
- [40] L. J. Allen, M. J. Brunger, I. E. McCarthy, and P. J. O. Teubner, *J. Phys. B* **20**, 4861 (1987).
- [41] M. J. Brunger, S. J. Buckman, L. J. Allen, I. E. McCarthy, and K. Ratnavelu, *J. Phys. B* **25**, 1823 (1992).
- [42] D. Goebel, U. Hohm, and G. Maroulis, *Phys. Rev. A* **54**, 1973 (1996).
- [43] O. Zatsarinny, K. Bartschat, G. Garcíá, F. Blanco, L. R. Hargreaves, D. B. Jones, R. Murrie, J. R. Brunton, M. J. Brunger, M. Hoshino, and S. J. Buckman, *Phys. Rev. A* **83**, 042702 (2011).
- [44] S. Chen, R. P. McEachran, and A. D. Stauffer, *J. Phys. B* **41**, 025201 (2008).
- [45] I. P. Grant, B. J. McKenzie, P. H. Norrington, D. F. Mayer, and N. C. Pyper, *Comput. Phys. Commun.* **21**, 207 (1980).
- [46] R. P. McEachran, D. L. Morgan, A. G. Ryman, and A. D. Stauffer, *J. Phys. B* **10**, 663 (1977).
- [47] R. P. McEachran, D. L. Morgan, A. G. Ryman, and A. D. Stauffer, *J. Phys. B* **11**, 951 (1978).
- [48] R. P. McEachran and A. D. Stauffer, *J. Phys. B* **23**, 4605 (1990).
- [49] K. Bartschat (private communication).
- [50] M. J. Brunger, *Int. Rev. Phys. Chem.* **36**, 333 (2017).
- [51] S. T. Perkins, D. E. Cullen, and S. M. Seltzer, LLNL Evaluated Electron Data Library, UCRL-50400 Vol. 31 (Lawrence Livermore National Laboratory, Livermore, California, 1991).
- [52] R. J. Zollweg, *J. Chem. Phys.* **50**, 4251 (1969).
- [53] K. Bartschat, O. Zatsarinny, I. Bray, D. V. Fursa, and A. T. Stelbovics, *J. Phys. B* **37**, 2617 (2004).
- [54] R. P. McEachran and A. D. Stauffer, *J. Phys. B* **25**, 1527 (1992).
- [55] M. Bartsch, H. Geesman, G. F. Hanne, and J. Kessler, *J. Phys. B* **25**, 1511 (1992).